Geophysical Research Letters®

The Impact of CO_2 and Climate State on Whether Dansgaard–Oeschger Type Oscillations Occur in Climate Models

Irene Malmierca-Vallet[1] , **Louise C. Sime[1]** , **Paul J. Valdes[2]** , **Marlene Klockmann[3]** , **Guido Vettoretti[4]** , **and John Slattery[1]**

[1]British Antarctic Survey, Cambridge, UK, [2]University of Bristol, Bristol, UK, [3]Universität Hamburg, Hamburg, Germany, [4]Niels Bohr Institute, University of Copenhagen, Copenhagen, Denmark

Abstract Greenland ice core records feature Dansgaard–Oeschger (D-O) events, which are abrupt warming episodes followed by gradual cooling during ice age climate. The three climate models used in this study (CCSM4, MPI-ESM, and HadCM3) show spontaneous self-sustained D-O-like oscillations (albeit with differences in amplitude, duration, and shape) in a remarkably similar, narrow window of carbon dioxide (CO_2) concentration, roughly 185–230 ppm. This range matches atmospheric CO_2 during Marine Isotopic Stage 3 (MIS 3: between 27.8 and 59.4 thousand of years BP, hereafter ka), a period when D-O events were most frequent. Insights from the three climate models point to North Atlantic (NA) sea-ice coverage as a key ingredient behind D-O type oscillations, which acts as a "tipping element." Other climate state properties such as Mean Atlantic Meridional Overturning Circulation strength, global mean temperature and salinity gradient in the Atlantic Ocean do not determine whether D-O type behavior can occur in all three models.

Plain Language Summary Dansgaard-Oeschger (D-O) events are sudden periods of warming followed by slow cooling during ice ages, as observed in Greenland's ice core records. The study used three different climate models to analyze these events, and all models showed similar behavior within a specific range of atmospheric carbon dioxide (CO_2) concentrations. This range of CO_2 concentrations aligns well with the levels found during the latter half of the last ice age when D-O events were most frequent. The study found that when CO_2 levels are outside this specific range, the climate models settle into one of two stable states, either warm with high CO_2 levels or cold with low CO_2 levels. These states are stable until CO_2 levels reach a certain "tipping point"- below around 185–195 ppm for the cold state and above around 217–230 ppm for the warm state. This study suggests that North Atlantic sea ice coverage is a crucial property essential for D-O like behavior to develop in complex climate models.

1. Introduction

The Marine Isotopic Stage 3 (MIS 3 — between 27.8 and 59.4 thousand of years BP, hereafter ka) was characterized by millennial-scale climate fluctuations, also known as Dansgaard-Oeschger (D-O) oscillations. During D-O events, atmospheric and oceanic conditions alternated between warm interstadial (of up to 10–16°C increase in air temperatures over Greenland) and cold stadial states (Dansgaard et al., 1993; Huber et al., 2006; Kindler et al., 2014). In the Southern Hemisphere, the climate transitions had a more gradual, lower-amplitude counterpart characterized by interhemispheric anti-phased variability related to the bipolar seesaw mechanism (Pedro et al., 2018; Stocker & Johnsen, 2003; Thompson et al., 2019). This climate variability over Antarctica shows a close resemblance to variations in atmospheric CO_2 (Barker & Knorr, 2007, 2016).

Paleoclimate records indicate that D-O events occurred when atmospheric CO_2 levels and global ice volume were intermediate between interglacial and glacial extremes (Barker et al., 2011; Bereiter et al., 2015; Dansgaard et al., 1993; Kawamura et al., 2017; McManus et al., 1999). During the MIS3, a period when D-O events were most frequent, atmospheric CO_2 levels declined from ~233 ppm around 60 ka until reaching a minimum of ~187.5 ppm around 25 ka (Bauska et al., 2021). Gradual variations in background climate, related to changes in atmospheric CO_2, may act as an indirect control on the occurrence, and stadial duration, of D-O events (Banderas et al., 2015; Li & Born, 2019; Vettoretti et al., 2022; Zhang et al., 2021). For example, the consecutive D-O events 5–7 show a reducing interstadial duration together with a cooling background linked to a gradual CO_2 reduction of ~15 ppm (Ahn & Brook, 2014; Dansgaard et al., 1993).

Malmierca-Vallet et al. (2023) review recent progress in modeling, and improvements to our understanding of the mechanisms behind D-O events. Several coupled atmosphere-ocean models have recently been able to reproduce D-O like oscillations, driven purely by internal feedbacks (Malmierca-Vallet et al., 2023). The prevalent hypotheses strongly link D-O events to variations in North Atlantic (NA) sea ice (Ando & Oka, 2021; Li & Born, 2019; Menviel et al., 2020; Sime et al., 2019; Vettoretti & Peltier, 2018), alongside variations in the strength of the Atlantic Meridional Overturning Circulation (AMOC; Li & Born, 2019; Lynch-Stieglitz, 2017), which itself is strongly connected to flows of heat and salinity in the NA (Ganopolski & Rahmstorf, 2001; Hu et al., 2008; Kageyama et al., 2012; Peltier & Vettoretti, 2014). Alongside D-O events as being primarily linked to oscillations in sea ice and AMOC, studies have also explored a variety of crucial D-O feedbacks including: how the subpolar gyre (SPG) couples to the key AMOC behaviors (Klockmann et al., 2020; Li & Born, 2019); how subsurface temperature change and salt advection feedbacks play key roles (Brown & Galbraith, 2016; Kuniyoshi et al., 2022); and how global scale salt feedbacks and oscillations help set key ocean properties (Armstrong et al., 2023; Peltier & Vettoretti, 2014).

Alongside recent progress on our understanding of key D-O mechanisms, Malmierca-Vallet et al. (2023) also help show that D-O like events can occur in model simulations under a range of boundary conditions. Seven General Circulation Models (GCMs) show D-O like oscillations under a variety of ice-sheet, atmospheric CO_2 and astronomical forcing boundary conditions. Vettoretti et al. (2022), Zhang et al. (2021) and Klockmann et al. (2018) explored how CO_2 forcing affects D-O like behavior; whilst Zhang et al. (2014) and Armstrong et al. (2023) explored the impacts of changes in Northern Hemisphere ice-sheet size. In particular, the Laurentide ice sheet (LIS) has been shown to play a key role behind millennial scale climate variability, highlighting the sensitivity of the climate system to land-ice extent.

The aim of this study is built on the work of Zhang et al. (2017); Vettoretti et al. (2022) and Malmierca-Vallet et al. (2023) in exploring both how well models simulate D-O events, and how CO_2 affects D-O like behavior in models. First, we explore how well the simulated D-O like behavior matches the known palaeo-record of D-O quantities. Second, we examine how D-O like behavior varies with CO_2 in models. Third, we look at whether there are common climate properties that characterize the oscillatory behavior in models.

2. Methods

2.1. Models and Simulations

We present results from three models, alongside measured NGRIP data (Figure 1). Given, prior to Malmierca-Vallet et al. (2023) there was no common D-O focused protocol, here we analyze results from an ensemble of opportunity. The existing simulations we could gather, which show D-O like behavior are run with three models: the Community Climate System Model Version 4 (CCSM4), which is part of the Community Earth System Model release version 1 (CESM1-CAM4); the Max Planck Institute Earth System Model (MPI-ESM); and the Bristol version of the Hadley Center Coupled Model 3 (HadCM3b). Each model uses boundary conditions which are intermediate between a pre-industrial (Eyring et al., 2016) and a Last Glacial Maximum (LGM) simulation (Kageyama et al., 2021). Whilst they do not all use the same ice sheet or insolation forcing, their CO_2 forcing covers the same range of values.

We use eight 8,000–10,000 years-long simulations run using the CCSM4 climate model (Peltier & Vettoretti, 2014). These use atmospheric CO_2 values from 170 to 240 ppm (Vettoretti et al., 2022) (Table S1 in Supporting Information S1). The ice sheet and insolation forcing are used from 21 ka. The ice sheet configuration is ICE-6G (Argus et al., 2014; Peltier et al., 2015). We use eight 4,000–12,350 years-long MPI-ESM simulations, which use atmospheric CO_2 from 149 to 353 ppm (Klockmann et al., 2018). These also use 21 ka insolation, alongside pre-industrial (PI) ice-sheets (Table S1 in Supporting Information S1). We also use 12 unpublished 4,700–10,000 years-long HadCM3 simulations. They are run with atmospheric CO_2 from 100 to 300 ppm (Table S1 in Supporting Information S1), with insolation and ice-sheets from 30 ka. In particular, the ICE-5G model (Peltier, 2004) is used to infer the 30 ka ice sheet configuration. ICE-5G simulates the evolution of ice extent, thickness and isostatic rebound up to the LGM, so the pre-LGM ice sheet is calculated from the equivalent sea level (ice volume), during the deglaciation. The same approach has been previously used in Armstrong et al. (2019) and Davies-Barnard et al. (2017). The full set of simulation output used here are freely available from the "Spontaneous Dansgaard-Oeschger type oscillations in climate models" project website: https://www.bas.ac.uk/project/sdoo/.
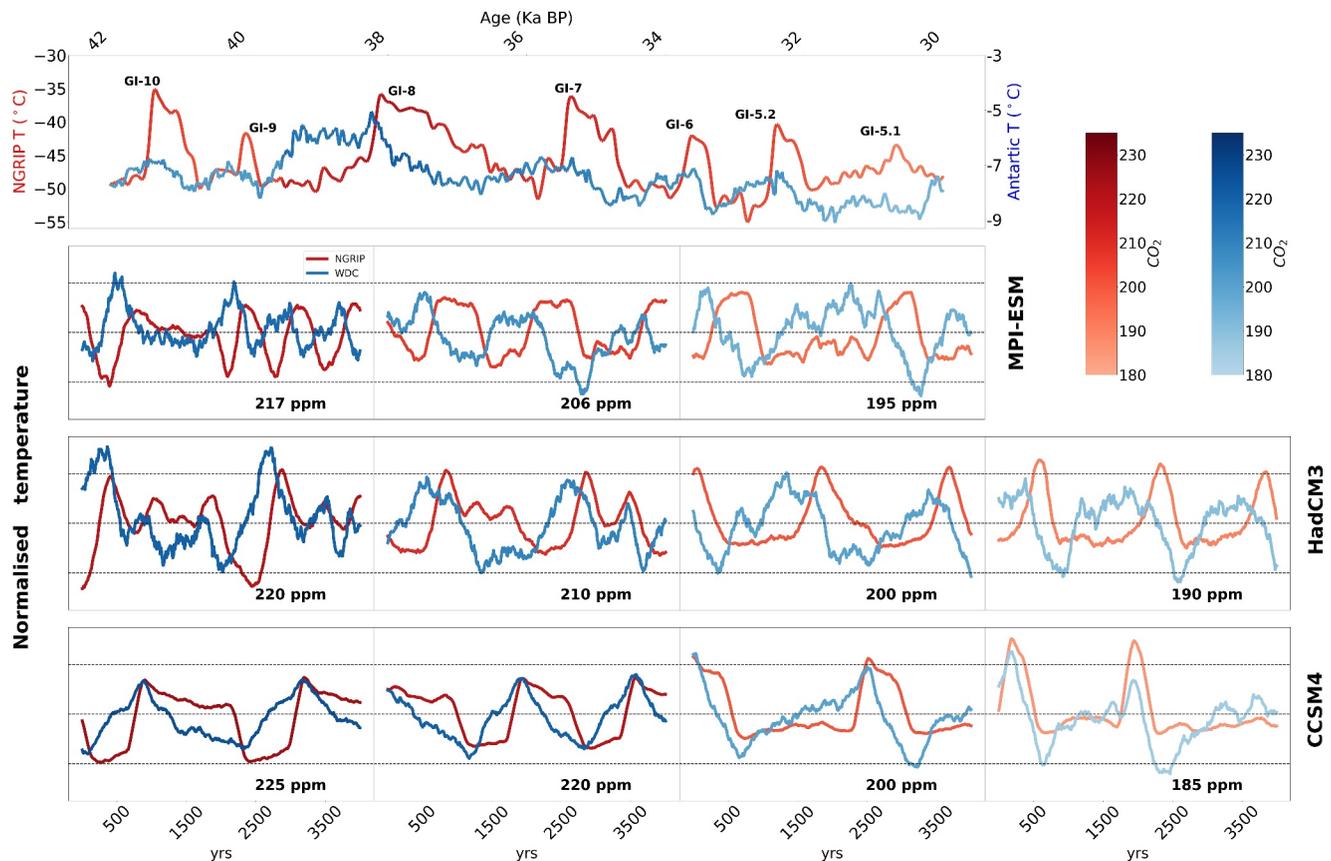
Figure 1. Measured and modeled D-O oscillations. (first row) MIS3 temperature reconstruction from North Greenland Ice Core Project (NGRIP) based on $\delta^{18}O$ and $\delta^{15}N$ records (Kindler et al., 2014; NGRIP Project Members, 2004). Stack of anomalous (relative to the past millennium) Antarctic Temperature based on δD and $\delta^{18}O$ records from six ice cores: EPICA Dronning Maud Land, EPICA Dome C, Talos Dome, Vostok, WAIS Divide Core (WDC) and Dome Fuji as published in Pedro et al. (2018). The NGRIP and Antarctic temperature time series are colored based on atmospheric CO_2 measurements from the WDC (Bauska et al., 2021). (second row) Max Planck Institute Earth System Model (third row) HadCM3 and (fourth row) CCSM4 time series of modeled surface air temperature at the grid points closest to the NGRIP (red) and WDC (blue) ice core sites. Modeled data is in time series of decadal average and smoothed with a 200-year running mean. For comparison, time series are normalized, and we select for each simulation time windows of 4,000 model-years where D-O cycles are most clear.

The MPI-ESM (Giorgetta et al., 2013; Stevens et al., 2013) and CCSM4 (Gettelman et al., 2012; Shields et al., 2012) atmosphere sub-models are run at $3.75 \times 3.75°$ and HadCM3 at a similar resolution of $3.75 \times 2.5°$ (Pope et al., 2000). They have 31, 26 and 19 atmospheric layers in the vertical respectively. The CCSM4 ocean model resolution is a nominal $3°$ irregular horizontal grid (referred to as ×3), with 60 vertical levels (Danabasoglu et al., 2012; Shields et al., 2012). Similarly, the ocean component of MPI-ESM has a nominal resolution of $3 \times 3°$, with 40 vertical levels (Jungclaus et al., 2006). The grid poles are located over Antarctica and Greenland. This configuration produces a 50–100 km resolution over the key subpolar NA region and a good realistic representation of deep convection (Klockmann et al., 2016, 2020). The HadCM3 ocean model resolution is $1.25 \times 1.25°$, on 20 vertical levels (Gordon et al., 2000). Further details of each model: physical core components, model denomination and description are in Gent et al. (2011) for CCSM4, Klockmann et al. (2018) for MPI-ESM and Valdes et al. (2017) for HadCM3.

Since the HadCM3 simulation run with 220 ppm does not show D-O type oscillations after around 4,500 model years (Figure S1h in Supporting Information S1), we analyze only the first 4,500 years of this particular simulation.

2.2. The Characterization of D-O Like Behavior in the Model Simulations

Klockmann et al. (2018) made use of AMOC variance (standard deviation), using time series of annual mean AMOC output, to both test for D-O like events and assess the proximity to a stability threshold (Armstrong

et al., 2017; Held & Kleinen, 2004; Kleinen et al., 2003; Tziperman, 2000). Similarly, we also apply this method, alongside a variation where we use the standard deviation of the NA average sea ice area (SIA) to establish D-O like oscillatory behavior (hereafter called "D-O index") for each individual simulation (Figure 2 and Figure S2 in Supporting Information S1).

In addition to characterizing if a simulation shows D-O like behavior, we wish to quantify the time spent in a stadial (vs. an interstadial) state. It is actually quite challenging to establish a common method to define inter-stadial/stadial phases that works for our three models and for all types of D-O like oscillations reproduced by each model. Figure 1 shows that (a) the D-O type oscillations in HadCM3 and MPI-ESM do not follow the classic sawtooth shape, (b) the amplitude of the D-O type oscillations widely differs within models, and (c) some MPI-ESM oscillations have a very short duration — of approximately 700–800 years. With this in mind and following previous studies (Alley et al., 2001; Ditlevsen et al., 2002, 2005; Lohmann & Ditlevsen, 2019; Mitsui & Crucifix, 2017), we define an upper and lower threshold (upper and lower dashed lines in Figure S3 in Supporting Information S1), when the AMOC index is five tenths standard deviation above and below the mean respectively to define time spent in an interstadial/stadial state (Figure S3 in Supporting Information S1). The transition from a stadial state to an interstadial state is defined by the first up-crossing of the upper threshold after up-crossing the lower threshold. In the same way, the transition from interstadial to stadial is defined by the first down-crossing of the lower threshold after down-crossing the upper threshold (For more details, see Figure S3 and schematic S3h in Supporting Information S1).

3. Results

3.1. Comparison Between D-O Records in Greenland Ice Cores and Simulated Behaviors

Based on ice core measurements, the amplitude of D-O events in Greenland temperature at NGRIP is estimated to be from +5 to +16.5°C ($\pm$3°C; Kindler et al., 2014). For MPI-ESM and HadCM3, the equivalent simulated amplitudes are 3.5 $\pm$ 0.4°C and 3.5 $\pm$ 0.8°C respectively, which fall at the lower end of the reconstructed range (Figure 1 and Figure S1 in Supporting Information S1). The CCSM4 model has a better match with observations, with 6.7 $\pm$ 0.5°C amplitudes (Figure 1 and Figure S1 in Supporting Information S1). In each case, the modeled surface temperature over Greenland is in phase with the simulated AMOC transport in the three models (Figure 1 and Figure S4 in Supporting Information S1).

In the three models, the oscillation frequency is in agreement with the D-O events in the ice core record, which show a characteristic periodicity ranging from 1,000 to 5,000 years (Boers et al., 2018; Buizert et al., 2015) (Figure 1 and Figure S1 in Supporting Information S1). Time series of surface air temperature from the grid point closest to NGRIP Greenland ice core site from the HadCM3, MPI-ESM and CCSM4 simulations show a similar to reality D-O event average periodicity of 1,584 $\pm$ 291, 1,406 $\pm$ 528 and 2,648 $\pm$ 1,446 years respectively (Figure 1 and Figure S1 in Supporting Information S1). Of the three, MPI-ESM shows some shorter D-O type oscillations (of approximately 700–800 model years).

D-O records in Greenland ice cores show that both stadials and interstadials vary in duration, from around a century to many millennia (Rasmussen et al., 2014). This is reproduced by the three models with a dominant stadial (interstadial) duration of approximately 1,166 $\pm$ 529 (750 $\pm$ 274), 739 $\pm$ 168 (516 $\pm$ 266), 671 $\pm$ 462 (475 $\pm$ 154) years in CCSM4, HadCM3 and MPI-ESM respectively (Figure 1 and Figure S1 in Supporting Information S1).

The NGRIP ice core shows that most of the longer MIS3 D-O events have a sawtooth shape: a rapid warming followed by slower cooling (Lohmann & Ditlevsen, 2019; Seager & Battisti, 2007) (Figure 1 and Figure S1 in Supporting Information S1). This shape is well reproduced by CCSM4. MPI-ESM and HadCM3, however, show a more symmetric rapid warming/rapid cooling waveform pattern. These simulated events are more consistent with some shorter DO events in observations, that is, D-O events 15, 10, 6, 5.2, and 4 which are characterized by a more symmetric shape (Buizert et al., 2015; Klockmann et al., 2020) (Figure 1).

3.2. Sea Ice, Salinity, and AMOC Variations in the Simulations

Two distinct NA sea-ice cover stable states are found in the three models; at low (high) CO_2 values, we find an increased (reduced) NA sea-ice cover stable state (Figure 2 and Figure S2 in Supporting Information S1). The NA sea-ice area for the ensemble mean of non-oscillatory experiments with low CO_2 concentrations (CO_2 values of

Figure 2.
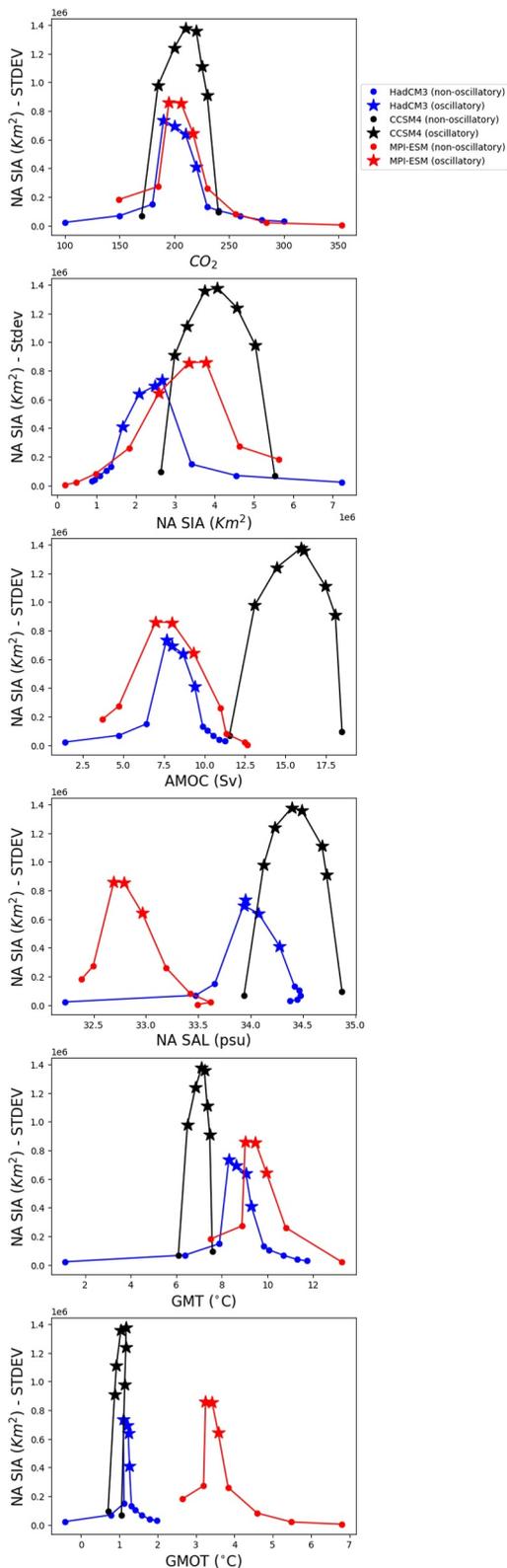
100–180 ppm for HadCM3, 149–185 ppm for MPI-ESM and 170 ppm for CCSM4) is 5.07 E + 06 km² in HadCM3, 5.53 E + 06 km² in CCSM4 and 5.13 E + 06 km² in MPI-ESM (Figure 2). In the high CO_2 stable state (CO_2 values of 230–300 ppm for HadCM3, 230–353 ppm for MPI-ESM and 230 ppm for CCSM4), the ensemble mean of NA sea-ice cover shrinks by 78% in HadCM3, 52.2% in CCSM4 and 82.9% in MPI-ESM compared to the low CO_2 (weak AMOC) stable state (Figure 2). While NA SIA fluctuates between interstadial and stadial phases, Arctic SIA is nearly constant between stadials and interstadials. For MPI-ESM, HadCM3 and CCSM4, the total NA sea-ice area stadial-interstadial (ensemble mean of all oscillatory simulations within each model) changes by 38.7%, 45%, 51.3%, whereas Arctic sea-ice area only changes by 3.3%, 3.6%, 0.7% respectively. This is because none of the simulations shows any significant region of summer sea ice free conditions in the Arctic. The largest difference between models is found in the Nordic Seas where SIA stadial-interstadial changes by 12% in MPI-ESM, 14% in HadCM3 and only 2.2% in CCSM4 (Figure S5 in Supporting Information S1).

There is strong evidence that NA sea ice coverage played a mayor role in D-O events (Jouzel et al., 2007; Masson-Delmotte et al., 2005; Sadatzki et al., 2019). During interstadial phases, the three models show an extensive retreat of sea ice in the eastern NA (Figure 3 and Figure S5 in Supporting Information S1) and there is an increase of deep convection in the Iceland basin, Irminger Sea and Nordic Seas compared to stadial phases (Figure 3). This is indicated by increases in mixed-layer depths (of more than 500 m in HadCM3 and MPI-ESM) and strong heat loss in the three models. Changes in mixed-layer depths are less pronounced in CCSM4, specially in the Nordic seas, most likely linked to sporadic deep convection, indicated by the shallower mixed-layer depths (Figure 3). In CCSM4, the reinvigoration of the AMOC across the stadial to interstadial transition primarily occurs in the Irminger Sea basin (Figure 3).

During interstadial phases, the three models show an extensive retreat of sea ice in the eastern NA (Figure 3 and Figure S5 in Supporting Information S1) and there is an increase of deep convection in the Iceland basin, Irminger Sea and Nordic Seas compared to stadial phases (Figure 3). This is indicated by increases in mixed-layer depths (of more than 500 m in HadCM3 and MPI-ESM) and strong heat loss in the three models. Changes in mixed-layer depths are less pronounced in CCSM4, specially in the Nordic seas, most likely linked to sporadic deep convection, indicated by the shallower mixed-layer depths (Figure 3). In CCSM4, the reinvigoration of the AMOC across the stadial to interstadial transition primarily occurs in the Irminger Sea basin (Figure 3).

Figure 2. Climate state properties, and the occurrence of D-O type behavior. (first row) Temporal variability of North Atlantic (NA) sea ice area (SIA) (km^2) as a function of CO_2 in HadCM3 (blue), Max Planck institute earth system model (MPI-ESM) (red) and CCSM4 (black). Also shown, temporal variability of NA SIA as a function of mean state (second row) NA SIA, (thrid row) AMOC, (fourth row) NA salinity, (fifth row) global mean temperature and (sixth row) global mean ocean temperature in HadCM3 (blue), MPI-ESM (red) and CCSM4 (black). We calculate variability as the standard deviation of the NA SIA time series. The time series are smoothed with a 100-year running mean and detrended before the calculation. Spin-up periods (~ first 1,000–2,000 years) are excluded. The model output is in time series of decadal average. The MPI-ESM sea ice concentration data is only available in 50-year average.

Ocean salinity in the three models display a prominent NA dipole pattern centered on the GIN Seas/SPG, and the tropics (Figure S6 in Supporting Information S1) (Armstrong et al., 2023; Klockmann et al., 2018, 2020; Vettoretti & Peltier, 2016, 2018). The contrasting pattern between these two regions during interstadial/stadial phases agrees with the salt oscillator hypothesis (Broecker et al., 1990). This suggests that this mechanism is present in the three models, and that the salinity gradient between the Northern NA (GIN Seas and SPG) and the tropics is an essential component of the D-O type oscillations (Armstrong et al., 2023; Klockmann et al., 2018, 2020; Vettoretti & Peltier, 2016, 2018). The results here emphasize the importance of the dynamics between the SPG and the tropics in generating the D-O type oscillations.

In the three models, the AMOC strength and thus the oscillations, are likely influenced by the salinity gradient between the subtropical and subpolar NA (Armstrong et al., 2023; Klockmann et al., 2018; Vettoretti & Peltier, 2016). The transition from a stadial into interstadial is associated with a subtropical-subpolar salinity difference above 1.13 ± 0.01 psu, 1.29 ± 0.02 psu and 0.52 ± 0.01 psu in MPI-ESM, HadCM3 and CCSM4 respectively (S7j). By contrast, the AMOC weakening is associated with a subtropical-subpolar salinity difference below 0.66 ± 0.03 psu in MPI-ESM and 0.46 ± 0.05 psu in HadCM3 and 0.05 ± 0.006 psu in CCSM4 (S7j). Although HadCM3 and MPI-ESM share similar salinity gradients, CCSM4 shows much smaller critical values.

A wide range of circulation proxies show that large-scale variations in the AMOC are in association with D-O events (Adkins et al., 1998; Gottschalk et al., 2015; Henry et al., 2016; Kissel et al., 2008; Lynch-Stieglitz, 2017; Piotrowski et al., 2005; Shackleton et al., 2000). Two distinct AMOC states are found in the three models; at high CO_2 levels, the AMOC is in a state with a strong and deep upper overturning cell (Figures S8b, S8e and S8h in Supporting Information S1). The overturning strength for the ensemble mean of non-oscillatory experiments with high CO_2 concentrations is of 16.5 Sv in HadCM3, 15 Sv in MPI-ESM and 18.4 Sv in CCSM4. In response to decreasing CO_2 levels, the AMOC shoals and weakens (Figures S8a, S8d and S8g in Supporting Information S1). Differences in the overturning strength between strong (high CO_2) and weak (low CO_2) AMOC states are of the order of up to 9.1 Sv in HadCM3, 8.9 Sv in MPI-ESM and 7.7 Sv in CCSM4 (Figures S8c, S8f and S8i in Supporting Information S1).

Ice and marine cores show that D-O events are characterized by anti-phased hemispheric behavior (Pedro et al., 2018; Stocker & Johnsen, 2003; Thompson et al., 2019). All three models show anti-phased hemispheric temperatures (over Antarctica and Greenland): all simulations show that interstadial (stadial) phases are characterized by a stronger (weaker) AMOC, warmer (cooler) Greenland surface temperatures, decrease (increase) NA sea ice coverage and increase (decrease) NA salinity (Figures 1 and 3, Figures S4 and S9 in Supporting Information S1).

3.3. CO_2 Controls on Modeled D-O Type Behavior

During MIS3, when atmospheric CO_2 varies between 233 and 187.5 ppm, there was a sequence of D-O events (Bauska et al., 2021). The atmospheric CO_2 range within which the three models show D-O like behavior agrees remarkably well — both with each other and with this actual MIS3 CO_2 (Figure 1 and Figure S9 in Supporting Information S1). Outside the D-O type oscillatory window, both at high and low CO_2 levels, the three models do not show D-O type oscillations (Figure S2 in Supporting Information S1). As CO_2 is reduced, D-O like behavior begins at 217–230 ppm in MPI-ESM, 220–230 ppm in HadCM3 and 230–240 ppm in CCSM4, respectively (Figure S2 in Supporting Information S1). Above this CO_2 level, the strong AMOC state is too stable to permit D-O like behavior. Below 195–185 ppm in MPI-ESM, 185–170 in CCSM4 and 190–180 ppm in HadCM3, D-O like behavior again stops, due to a weak but stable AMOC (Figure S2 in Supporting Information S1). In general, D-O like behavior occurs when AMOC states are marginally unstable, and oscillations in AMOC can occur (Colin de Verdière, 2007).

We look at how D-O like behavior, characterized using our D-O index, varies with the following climate properties: NA sea-ice, NA salinity, mean AMOC strength, Global mean Ocean temperature (GMOT) Global mean temperature (GMT), salinity gradient and subsurface temperature change (Figure 2 and Figure S13 in Supporting Information S1). Of these climate properties, the models show that our D-O index shows the most overlap in NA sea ice for the three models (Figure 2b): the three models oscillate in a similar window of NA SIA. D-O like behavior is associated with SIA between approximately $1.38 - 5.53$ E $+ 06$ km^2. More precisely, D-O like behavior occur when SIA is above $1.38 - 1.67$ E $+ 06$ km^2 in HadCM3, $2.64 - 2.99$ E $+ 06$ km^2 in CCSM4 and $1.83 - 2.58$ E $+ 06$ km^2 in MPI-ESM; and SIA is below $2.67 - 3.41$ E $+ 06$ km^2 in HadCM3,
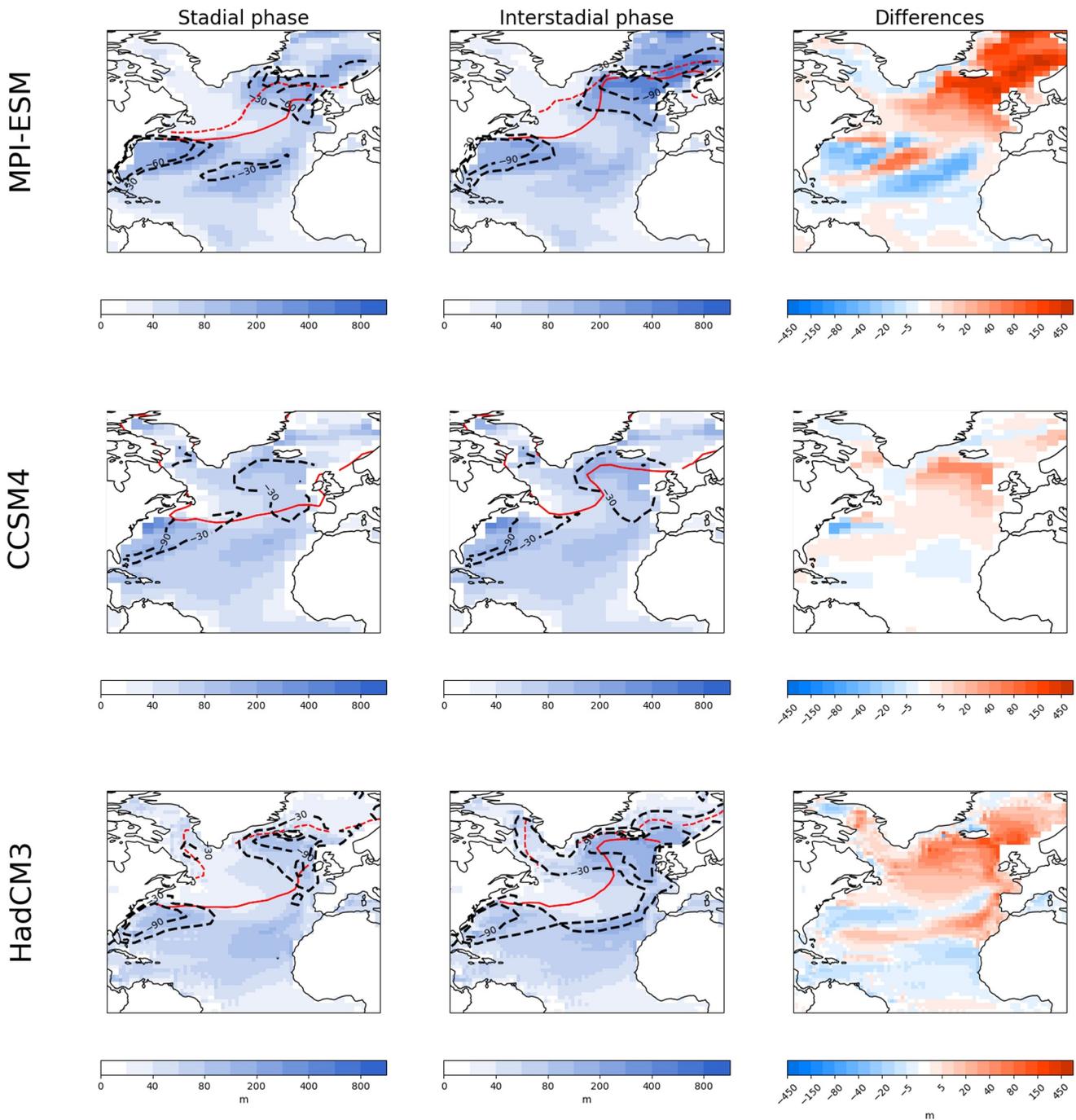
Figure 3. Mean mixed-layer depth (shading), net heat flux (black dashed line) and sea ice edge in March (solid red line) and September (dashed red line) during stadial (first column) and interstadial (second column) phases in Max Planck Institute Earth System Model (first row), CCSM4 (second row) and HadCM3 (third row). The sea ice edges are defined as the 15% contour sea ice cover. Modeled CCSM4 data is only available in time series of decadal average, and therefore the red solid line represents the annual sea ice edge.

$5.04 - 5.53 \, \mathrm{E} + 06 \, \mathrm{km}^2$ in CCSM4 and $3.78 - 4.63 \, \mathrm{E} + 06 \, \mathrm{km}^2$ in MPI-ESM. In addition, we find that the three models share a similar critical SIA variability threshold (Figure 2b): differences in NA SIA between strong (high CO_2) and weak (low CO_2) AMOC stable states are of the order of $1.5 \, \mathrm{E} + 06 \, \mathrm{km}^2$, $2.5 \, \mathrm{E} + 06 \, \mathrm{km}^2$ and $2.0 \, \mathrm{E} + 06 \, \mathrm{km}^2$ in HadCm3, CCSM4 and MPI-ESM respectively.

It is most intriguing that none of the other climate properties: NA salinity, mean AMOC strength, GMOT, GMT, salinity gradient and subsurface temperature change show commonality in their impact on our D-O index between the models (Figure 2 and Figure S13 in Supporting Information S1). At its most basic, this shows that none of these other properties directly controls whether D-O type behavior can occur. Rather, a particular NA SIA is the only property that may be necessary for D-O like behavior to manifest in GCMs.

It is difficult to determine what controls DO-type behavior in GCMs. Nevertheless, a number of modeling studies have showed that stadial phases are characterized by less northward transport of salt and therefore a build-up of salty warm water in the low-latitude NA (Pedro et al., 2018; Peltier & Vettoretti, 2014). Here, we examine, whether CO_2 could exert control on low-latitude NA salinity build-up in the upper ocean. CCSM4 shows a decrease (increase) of salinity in the low-latitude NA during stadial (interstadial) phases in the experiments with lower CO_2 compared to the ensemble mean (Figures S10 and S11 in Supporting Information S1). The converse seems to be true at higher CO_2 levels, albeit the 225 ppm CCSM4 simulation which shows less contrasting changes between stadials and interstadials (Figures S10 and S11 in Supporting Information S1). In the case of HadCM3 and MPI-ESM, we do not find an obvious distinct response to CO_2 between stadial and interstadial phases. Both models show an increased build-up of salinity and warm waters in the mid-latitude NA either during stadials or interstadial phases for the experiments with higher CO_2 compared to the ensemble mean (Figures S10 and S11 in Supporting Information S1). Based on these results, it is difficult to draw a firm conclusion on the role of CO_2 on low-latitude NA salinity build-up in the upper ocean. Further sensitivity CO_2 simulations run with other GCMs and complementary analysis would be most useful to check if these are robust features.

4. Conclusions

We analyzed simulations which show D-O type behavior under a 21 ka orbital set-up configuration used in MPI-ESM and CCMS4, and for a 30 ka orbital set-up for HadCM3. The LGM, PI and intermediate (MIS3-like) ice sheet configurations used across the three models here are all conducive to D-O like behavior. Any of these orbital configurations and ice sheet morphologies can generate a glacial climate background state under which the AMOC spontaneously oscillates. NH ice sheet changes have multiple impacts on the oceans and sea ice, including on NA wind stress, oceanic gateways and can modulate the NA freshwater and density budget, and therefore also the AMOC stability (Hu et al., 2012, Figure 5 in Malmierca-Vallet, Sime and D-O community, 2023). The impact of Earth's orbital parameters in D-O type oscillations is also known to be important. Stadial and interstadial lengths are also affected by the impacts of (a) climatic precession on boreal summer insolation and (b) obliquity reduction in high-latitude mean annual insolation (Kuniyoshi et al., 2022; Zhang et al., 2021).

The three climate models used in this study (CCSM4, HadCM3 and MPI-ESM) show D-O like behavior at CO_2 levels, which match when MIS3 D-O events actually occurred. Outside the D-O type oscillatory window, both at low (weak AMOC) and high (strong AMOC) CO_2 levels, the three models do not show D-O type oscillations (Figure S2 in Supporting Information S1).

The three models reproduce D-O type behavior in a similar range of NA SIA between approx $1.38 - 5.53 \, \mathrm{E} + 06 \, \mathrm{km}^2$. No other climate properties (such as NA salinity, mean AMOC strength, GMOT, GMT, salinity gradient in the Atlantic Ocean and subsurface temperature changes) seem to directly control whether D-O type behavior can happen. That is, NA SIA seems to be the only property that may be necessary for D-O like behavior to develop in GCMs. To establish this, and in what ways other climate properties interact in determining whether simulations oscillate, it would be most helpful to have a set of simulations run using common MIS3 boundary conditions (Malmierca-Vallet et al., 2023).

It remains to be understood why such D-O type oscillations are not present in all simulations with intermediate (glacial-interglacial) boundary conditions (Guo et al., 2019; Zhang & Prange, 2020). This suggests a "sweet spot," where the system is more susceptible to unforced oscillatory behavior. We show here that the presence of D-O type oscillations in MPI-ESM, CCSM4 and HadCM3 are sensitive to the levels of background atmospheric CO_2 and NA SIA, allowing a salt oscillator mode to develop, where oscillations can be maintained by feedbacks within the system.

In summary, the three models show a narrow window of atmospheric CO_2 concentrations (~185–230 ppm) bounding a D-O sweet spot, which matches the CO_2 range under which D-O events occurred during MIS3. The time between climate transitions is determined by temporal variations in the state of the atmosphere, ocean and

sea ice, with CO_2 acting as a control on the rate of approach to the climate tipping point. Results from the three climate models point to NA sea-ice coverage as an essential climate property for D-O type oscillatory behavior to develop in GCMs. Sea ice plays a major role in triggering the interstadials (stadials) by conditioning the SPG (i.e., intensifying (weakening) respectively). It is important to note that the range of atmospheric CO_2 bounding the D–O window identified in this study may change or even dissipate under different boundary conditions. D-O oscillations are also sensitive to changes in Earth's orbital configuration (Zhang et al., 2021) and NH ice sheet shapes (Armstrong et al., 2023; Zhang et al., 2014), which has been shown to alter glacial NA sea ice cover and atmospheric and ocean circulation patterns. Deep energetic mixing in the ocean and increased tidal forcing may also modulate D-O oscillations (Schmittner et al., 2015). Thus, further investigation of the uncertainty associated with these other mechanisms described here, particularly starting from a common D-O protocol (Malmierca-Vallet et al., 2023) would be very useful to (a) better investigate how atmospheric CO_2 actually helps control this D–O sweet spot and (b) test whether higher resolution models show similar feedbacks–and similar D-O type behaviors–and how more realistic flows through Arctic straits could influence key D-O relative feedbacks.

Data Availability Statement

Simulations were carried out using three models: (a) the Community Climate System Model Version 4 (CCSM4), (b) the MPI-ESM, and (c) the Bristol version of the Hadley Centre Coupled Model 3 (HadCM3b). The CCSM4 model output is available through Vettoretti et al., 2022 and the MPI-ESM model output is available through Klockmann et al., 2018; Klockmann et al., 2020. The HadCM3 model data is available through Malmierca-Vallet et al., 2024 under the Open Government License (http://www.nationalarchives.gov.uk/doc/open-government-licence/version/3/). Observation data sets for this research are included in Pedro et al., 2018; Bauska et al., 2021.

References

Adkins, J. F., Cheng, H., Boyle, E. A., Druffel, E. R., & Edwards, R. L. (1998). Deep-sea coral evidence for rapid change in ventilation of the deep North Atlantic 15,400 years ago. *Science*, *280*(5364), 725–728. https://doi.org/10.1126/science.280.5364.725

Ahn, J., & Brook, E. J. (2014). Siple dome ice reveals two modes of millennial CO_2 change during the last ice age. *Nature Communications*, *5*(1), 3723. https://doi.org/10.1038/ncomms4723

Alley, R., Anandakrishnan, S., & Jung, a. P. (2001). Stochastic resonance in the north Atlantic. *Paleoceanography*, *16*(2), 190–198. https://doi.org/10.1029/2000pa000518

Ando, T., & Oka, A. (2021). Hysteresis of the glacial Atlantic meridional overturning circulation controlled by thermal feedbacks. *Geophysical Research Letters*, *48*(24), e2021GL095809. https://doi.org/10.1029/2021gl095809

Argus, D. F., Peltier, W., Drummond, R., & Moore, A. W. (2014). The Antarctica component of postglacial rebound model ice-6g_c (vm5a) based on GPS positioning, exposure age dating of ice thicknesses, and relative sea level histories. *Geophysical Journal International*, *198*(1), 537–563. https://doi.org/10.1093/gji/ggu140

Armstrong, E., Hopcroft, P. O., & Valdes, P. J. (2019). A simulated northern hemisphere terrestrial climate dataset for the past 60,000 years. *Scientific Data*, *6*(1), 1–16. https://doi.org/10.1038/s41597-019-0277-1

Armstrong, E., Izumi, K., & Valdes, P. (2023). Identifying the mechanisms of do-scale oscillations in a GCM: A salt oscillator triggered by the Laurentide ice sheet. *Climate Dynamics*, *60*(11), 3983–4001. https://doi.org/10.1007/s00382-022-06564-y

Armstrong, E., Valdes, P., House, J., & Singarayer, J. (2017). Investigating the impact of CO_2 on low-frequency variability of the AMOC in HADCM3. *Journal of Climate*, *30*(19), 7863–7883. https://doi.org/10.1175/jcli-d-16-0767.1

Banderas, R., Alvarez-Solas, J., Robinson, A., & Montoya, M. (2015). An interhemispheric mechanism for glacial abrupt climate change. *Climate Dynamics*, *44*(9–10), 2897–2908. https://doi.org/10.1007/s00382-014-2211-8

Barker, S., & Knorr, G. (2007). Antarctic climate signature in the Greenland ice core record. *Proceedings of the National Academy of Sciences*, *104*(44), 17278–17282. https://doi.org/10.1073/pnas.0708494104

Barker, S., & Knorr, G. (2016). A paleo-perspective on the AMOC as a tipping element. *PAGES Magazine*, *24*(1), 14–15. https://doi.org/10.22498/pages.24.1.14

Barker, S., Knorr, G., Edwards, R. L., Parrenin, F., Putnam, A. E., Skinner, L. C., et al. (2011). 800,000 years of abrupt climate variability. *Science*, *334*(6054), 347–351. https://doi.org/10.1126/science.1203580

Bauska, T. K., Marcott, S. A., & Brook, E. J. (2021). Abrupt changes in the global carbon cycle during the last glacial period. *Nature Geoscience*, *14*(2), 91–96. https://doi.org/10.1038/s41561-020-00680-2

Bereiter, B., Eggleston, S., Schmitt, J., Nehrbass-Ahles, C., Stocker, T. F., Fischer, H., et al. (2015). Revision of the epica dome c CO_2 record from 800 to 600 kyr before present. *Geophysical Research Letters*, *42*(2), 542–549. https://doi.org/10.1002/2014gl061957

Boers, N., Ghil, M., & Rousseau, D.-D. (2018). Ocean circulation, ice shelf, and sea ice interactions explain Dansgaard–Oeschger cycles. *PNAS*, *115*(47), E11005–E11014. https://doi.org/10.1073/pnas.1802573115

Broecker, W. S., Bond, G., Klas, M., Bonani, G., & Wolfli, W. (1990). A salt oscillator in the glacial Atlantic? 1. The concept. *Paleoceanography*, *5*(4), 469–477. https://doi.org/10.1029/pa005i004p00469

Brown, N., & Galbraith, E. D. (2016). Hosed vs. unhosed: Interruptions of the Atlantic meridional overturning circulation in a global coupled model, with and without freshwater forcing. *Climate of the Past*, *12*(8), 1663–1679. https://doi.org/10.5194/cp-12-1663-2016

Buizert, C., Adrian, B., Ahn, J., Albert, M., Alley, R. B., Baggenstos, D., et al. (2015). Precise interpolar phasing of abrupt climate change during the last ice age. *Nature*, *520*(7549), 661–665. https://doi.org/10.1038/nature14401

Colin de Verdière, A. (2007). A simple model of millennial oscillations of the thermohaline circulation. *Journal of Physical Oceanography*, *37*(5), 1142–1155. https://doi.org/10.1175/jpo3056.1

Danabasoglu, G., Bates, S. C., Briegleb, B. P., Jayne, S. R., Jochum, M., Large, W. G., et al. (2012). The CCSM4 ocean component. *Journal of Climate*, *25*(5), 1361–1389. https://doi.org/10.1175/jcli-d-11-00091.1

Dansgaard, W., Johnsen, S. J., Clausen, H. B., Dahl-Jensen, D., Gundestrup, N., Hammer, C., et al. (1993). Evidence for general instability of past climate from a 250-kyr ice-core record. *Nature*, *364*(6434), 218–220. https://doi.org/10.1038/364218a0

Davies-Barnard, T., Ridgwell, A., Singarayer, J., & Valdes, P. (2017). Quantifying the influence of the terrestrial biosphere on glacial–interglacial climate dynamics. *Climate of the Past*, *13*(10), 1381–1401. https://doi.org/10.5194/cp-13-1381-2017

Ditlevsen, P. D., Ditlevsen, S., & Andersen, K. K. (2002). The fast climate fluctuations during the statial and interstadial climate states. *Annals of Glaciology*, *35*, 457–462. https://doi.org/10.3189/172756402781816870

Ditlevsen, P. D., Kristensen, M. S., & Andersen, K. K. (2005). The recurrence time of Dansgaard-Oeschger events and limits on the possible periodic component. *Journal of Climate*, *18*(14), 2594–2603. https://doi.org/10.1175/jcli3437.1

Eyring, V., Bony, S., Meehl, G. A., Senior, C. A., Stevens, B., Stouffer, R. J., & Taylor, K. E. (2016). Overview of the coupled model inter-comparison project phase 6 (CMIP6) experimental design and organization. *Geoscientific Model Development*, *9*(5), 1937–1958. https://doi.org/10.5194/gmd-9-1937-2016

Ganopolski, A., & Rahmstorf, S. (2001). Rapid changes of glacial climate simulated in a coupled climate model. *Nature*, *409*(6817), 153–158. https://doi.org/10.1038/35051500

Gent, P. R., Danabasoglu, G., Donner, L. J., Holland, M. M., Hunke, E. C., Jayne, S. R., et al. (2011). The community climate system model version 4. *Journal of Climate*, *24*(19), 4973–4991. https://doi.org/10.1175/2011jcli4083.1

Gettelman, A., Kay, J., & Shell, K. (2012). The evolution of climate sensitivity and climate feedbacks in the community atmosphere model. *Journal of Climate*, *25*(5), 1453–1469. https://doi.org/10.1175/jcli-d-11-00197.1

Giorgetta, M. A., Jungclaus, J., Reick, C. H., Legutke, S., Bader, J., Böttinger, M., et al. (2013). Climate and carbon cycle changes from 1850 to 2100 in MPI-ESM simulations for the coupled model intercomparison project phase 5. *Journal of Advances in Modeling Earth Systems*, *5*(3), 572–597. https://doi.org/10.1002/jame.20038

Gordon, C., Cooper, C., Senior, C. A., Banks, H., Gregory, J. M., Johns, T. C., et al. (2000). The simulation of SST, sea ice extents and ocean heat transports in a version of the hadley centre coupled model without flux adjustments. *Climate Dynamics*, *16*(2–3), 147–168. https://doi.org/10.1007/s003820050010

Gottschalk, J., Skinner, L. C., Misra, S., Waelbroeck, C., Menviel, L., & Timmermann, A. (2015). Abrupt changes in the southern extent of north Atlantic deep water during Dansgaard–Oeschger events. *Nature Geoscience*, *8*(12), 950–954. https://doi.org/10.1038/ngeo2558

Guo, C., Nisancioglu, K. H., Bentsen, M., Bethke, I., & Zhang, Z. (2019). Equilibrium simulations of marine isotope stage 3 climate. *Climate of the Past*, *15*(3), 1133–1151. https://doi.org/10.5194/cp-15-1133-2019

Held, H., & Kleinen, T. (2004). Detection of climate system bifurcations by degenerate fingerprinting. *Geophysical Research Letters*, *31*(23). https://doi.org/10.1029/2004gl020972

Henry, L., McManus, J., Curry, W., Roberts, N., Piotrowski, A., & Keigwin, L. (2016). North Atlantic Ocean circulation and abrupt climate change during the last glaciation. *Science*, *353*(6298), 470–474. https://doi.org/10.1126/science.aaf5529

Hu, A., Meehl, G. A., Han, W., Timmermann, A., Otto-Bliesner, B., Liu, Z., et al. (2012). Role of the Bering Strait on the hysteresis of the ocean conveyor belt circulation and glacial climate stability. *Proceedings of the National Academy of Sciences*, *109*(17), 6417–6422. https://doi.org/10.1073/pnas.1116014109

Hu, A., Otto-Bliesner, B. L., Meehl, G. A., Han, W., Morrill, C., Brady, E. C., & Briegleb, B. (2008). Response of thermohaline circulation to freshwater forcing under present-day and LGM conditions. *Journal of Climate*, *21*(10), 2239–2258. https://doi.org/10.1175/2007jcli1985.1

Huber, C., Leuenberger, M., Spahni, R., Flückiger, J., Schwander, J., Stocker, T. F., et al. (2006). Isotope calibrated Greenland temperature record over marine isotope stage 3 and its relation to ch4. *Earth and Planetary Science Letters*, *243*(3–4), 504–519. https://doi.org/10.1016/j.epsl.2006.01.002

Jouzel, J., Masson-Delmotte, V., Cattani, O., Dreyfus, G., Falourd, S., Hoffmann, G., et al. (2007). Orbital and millennial antarctic climate variability over the past 800,000 years. *Science*, *317*(5839), 793–796. https://doi.org/10.1126/science.1141038

Jungclaus, J. H., Keenlyside, N., Botzet, M., Haak, H., Luo, J.-J., Latif, M., et al. (2006). Ocean circulation and tropical variability in the coupled model ECHAM5/MPI-OM. *Journal of Climate*, *19*(16), 3952–3972. https://doi.org/10.1175/jcli3827.1

Kageyama, M., Harrison, S. P., Kapsch, M.-L., Lofverstrom, M., Lora, J. M., Mikolajewicz, U., et al. (2021). The pmip4 last glacial maximum experiments: Preliminary results and comparison with the pmip3 simulations. *Climate of the Past*, *17*(3), 1065–1089. https://doi.org/10.5194/cp-17-1065-2021

Kageyama, M., Merkel, U., Otto-Bliesner, B., Prange, M., Abe-Ouchi, A., Lohmann, G., et al. (2012). Climatic impacts of fresh water hosing under last glacial maximum conditions: A multi-model study. *Climate of the Past Discussions*, *8*(4).

Kawamura, K., Abe-Ouchi, A., Motoyama, H., Ageta, Y., Aoki, S., Azuma, N., et al. (2017). State dependence of climatic instability over the past 720,000 years from antarctic ice cores and climate modeling. *Science Advances*, *3*(2), e1600446. https://doi.org/10.1126/sciadv.1600446

Kindler, P., Guillevic, M., Baumgartner, M. F., Schwander, J., Landais, A., & Leuenberger, M. (2014). Temperature reconstruction from 10 to 120 kyr b2k from the ngrip ice core. *Climate of the Past*, *10*(2), 887–902. https://doi.org/10.5194/cp-10-887-2014

Kissel, C., Laj, C., Piotrowski, A. M., Goldstein, S. L., & Hemming, S. R. (2008). Millennial-scale propagation of Atlantic deep waters to the glacial southern ocean. *Paleoceanography*, *23*(2). https://doi.org/10.1029/2008pa001624

Kleinen, T., Held, H., & Petschel-Held, G. (2003). The potential role of spectral properties in detecting thresholds in the earth system: Application to the thermohaline circulation. *Ocean Dynamics*, *53*(2), 53–63. https://doi.org/10.1007/s10236-002-0023-6

Klockmann, M., Mikolajewicz, U., Kleppin, H., & Marotzke, J. (2020). Coupling of the subpolar gyre and the overturning circulation during abrupt glacial climate transitions. *Geophysical Research Letters*, *47*(21), e2020GL090361. https://doi.org/10.1029/2020GL090361

Klockmann, M., Mikolajewicz, U., & Marotzke, J. (2016). The effect of greenhouse gas concentrations and ice sheets on the glacial AMOC in a coupled climate model. *Climate of the Past*, *12*(9), 1829–1846. https://doi.org/10.5194/cp-12-1829-2016

Klockmann, M., Mikolajewicz, U., & Marotzke, J. (2018). Two AMOC states in response to decreasing greenhouse gas concentrations in the coupled climate model MPI-ESM. *Journal of Climate*, *31*(19), 7969–7984. https://doi.org/10.1175/JCLI-D-17-0859.1

Kuniyoshi, Y., Abe-Ouchi, A., Sherriff-Tadano, S., Chan, W.-L., & Saito, F. (2022). Effect of climatic precession on Dansgaard-Oeschger-like oscillations. *Geophysical Research Letters*, *49*(6), e2021GL095695. https://doi.org/10.1029/2021gl095695

Li, C., & Born, A. (2019). Coupled atmosphere-ice-ocean dynamics in Dansgaard-Oeschger events. *Quaternary Science Reviews*, *203*, 1–20. https://doi.org/10.1016/j.quascirev.2018.10.031

Lohmann, J., & Ditlevsen, P. (2019). Objective extraction and analysis of statistical features of Dansgaard-Oeschger events. *Climate of the Past*, *15*(5), 1771–1792. https://doi.org/10.5194/cp-15-1771-2019

Lynch-Stieglitz, J. (2017). The Atlantic meridional overturning circulation and abrupt climate change. *Annual Review of Marine Science*, *9*(1), 83–104. https://doi.org/10.1146/annurev-marine-010816-060415

Malmierca-Vallet, I., Sime, L. C., & The D-O community. (2023). Dansgaard–Oeschger events in climate models: Review and baseline marine isotope stage 3 (MIS3) protocol. *Climate of the Past*, *19*(5), 915–942. https://doi.org/10.5194/cp-19-915-2023

Malmierca-Vallet, I., Sime, L. C., Valdes, P. J., Klockmann, M., Vettoretti, G., & Slattery, J. (2024). Hadcm3 model outputs: Spontaneous Dansgaard-Oeschger type oscillations (version 1.0). [Dataset]. NERC EDS UK Polar Data Centre. https://doi.org/10.5285/92B07757-3897-4A26-B93D-C508FFE93846

Masson-Delmotte, V., Jouzel, J., Landais, A., Stievenard, M., Johnsen, S., White, J., et al. (2005). Grip deuterium excess reveals rapid and orbital-scale changes in Greenland moisture origin. *Science*, *309*(5731), 118–121. https://doi.org/10.1126/science.1108575

McManus, J. F., Oppo, D. W., & Cullen, J. L. (1999). A 0.5-million-year record of millennial-scale climate variability in the north Atlantic. *Science*, *283*(5404), 971–975. https://doi.org/10.1126/science.283.5404.971

Menviel, L. C., Skinner, L. C., Tarasov, L., & Tzedakis, P. C. (2020). An ice–climate oscillatory framework for Dansgaard–Oeschger cycles. *Nature Reviews Earth and Environment*, *1*(12), 677–693. https://doi.org/10.1038/s43017-020-00106-y

Mitsui, T., & Crucifix, M. (2017). Influence of external forcings on abrupt millennial-scale climate changes: A statistical modelling study. *Climate Dynamics*, *48*(7), 2729–2749. https://doi.org/10.1007/s00382-016-3235-z

NGRIP Project Members. (2004). High-resolution record of northern hemisphere climate extending into the last interglacial period. *Nature*, *431*(7005), 147–151. https://doi.org/10.1038/nature02805

Pedro, J. B., Jochum, M., Buizert, C., He, F., Barker, S., & Rasmussen, S. O. (2018). Beyond the bipolar seesaw: Toward a process understanding of interhemispheric coupling. *Quaternary Science Reviews*, *192*, 27–46. https://doi.org/10.1016/j.quascirev.2018.05.005

Peltier, W. R. (2004). Global glacial isostasy and the surface of the ice-age earth: The ice-5g (vm2) model and grace. *Annual Review of Earth and Planetary Sciences*, *32*(1), 111–149. https://doi.org/10.1146/annurev.earth.32.082503.144359

Peltier, W. R., Argus, D., & Drummond, R. (2015). Space geodesy constrains ice age terminal deglaciation: The global ice-6g_c (vm5a) model. *Journal of Geophysical Research: Solid Earth*, *120*(1), 450–487. https://doi.org/10.1002/2014jb011176

Peltier, W. R., & Vettoretti, G. (2014). Dansgaard-Oeschger oscillations predicted in a comprehensive model of glacial climate: A "kicked" salt oscillator in the Atlantic. *Geophysical Research Letters*, *41*(20), 7306–7313. https://doi.org/10.1002/2014gl061413

Piotrowski, A. M., Goldstein, S. L., Hemming, S. R., & Fairbanks, R. G. (2005). Temporal relationships of carbon cycling and ocean circulation at glacial boundaries. *Science*, *307*(5717), 1933–1938. https://doi.org/10.1126/science.1104883

Pope, V., Gallani, M., Rowntree, P., & Stratton, R. (2000). The impact of new physical parametrizations in the Hadley centre climate model: Hadam3. *Climate Dynamics*, *16*(2–3), 123–146. https://doi.org/10.1007/s003820050009

Rasmussen, S. O., Bigler, M., Blockley, S. P., Blunier, T., Buchardt, S. L., Clausen, H. B., et al. (2014). A stratigraphic framework for abrupt climatic changes during the last glacial period based on three synchronized Greenland ice-core records: Refining and extending the intimate event stratigraphy. *Quaternary Science Reviews*, *106*, 14–28. https://doi.org/10.1016/j.quascirev.2014.09.007

Sadatzki, H., Dokken, T. M., Berben, S. M., Muschitiello, F., Stein, R., Fahl, K., et al. (2019). Sea ice variability in the southern Norwegian sea during glacial Dansgaard-Oeschger climate cycles. *Science Advances*, *5*(3), eaau6174. https://doi.org/10.1126/sciadv.aau6174

Schmittner, A., Green, J., & Wilmes, S.-B. (2015). Glacial ocean overturning intensified by tidal mixing in a global circulation model. *Geophysical Research Letters*, *42*(10), 4014–4022. https://doi.org/10.1002/2015gl063561

Seager, R., & Battisti, D. S. (2007). Challenges to our understanding of the general circulation: Abrupt climate change. *Global Circulation of the Atmosphere*, 331–371.

Shackleton, N. J., Hall, M. A., & Vincent, E. (2000). Phase relationships between millennial-scale events 64,000–24,000 years ago. *Paleoceanography*, *15*(6), 565–569. https://doi.org/10.1029/2000pa000513

Shields, C. A., Bailey, D. A., Danabasoglu, G., Jochum, M., Kiehl, J. T., Levis, S., & Park, S. (2012). The low-resolution ccsm4. *Journal of Climate*, *25*(12), 3993–4014. https://doi.org/10.1175/jcli-d-11-00260.1

Sime, L. C., Hopcroft, P. O., & Rhodes, R. H. (2019). Impact of abrupt sea ice loss on Greenland water isotopes during the last glacial period. *PNAS*, *116*(10), 4099–4104. https://doi.org/10.1073/pnas.1807261116

Stevens, B., Giorgetta, M., Esch, M., Mauritsen, T., Crueger, T., Rast, S., et al. (2013). Atmospheric component of the MPI-M earth system model: Echam6. *Journal of Advances in Modeling Earth Systems*, *5*(2), 146–172. https://doi.org/10.1002/jame.20015

Stocker, T. F., & Johnsen, S. J. (2003). A minimum thermodynamic model for the bipolar seesaw. *Paleoceanography*, *18*(4). https://doi.org/10.1029/2003pa000920

Thompson, A. F., Hines, S. K., & Adkins, J. F. (2019). A southern ocean mechanism for the interhemispheric coupling and phasing of the bipolar seesaw. *Journal of Climate*, *32*(14), 4347–4365. https://doi.org/10.1175/jcli-d-18-0621.1

Tziperman, E. (2000). Proximity of the present-day thermohaline circulation to an instability threshold. *Journal of Physical Oceanography*, *30*(1), 90–104. https://doi.org/10.1175/1520-0485(2000)030<0090:potpdt>2.0.co;2

Valdes, P. J., Armstrong, E., Badger, M. P., Bradshaw, C. D., Bragg, F., Crucifix, M., et al. (2017). The bridge hadcm3 family of climate models: Hadcm3@ Bristol v1. 0. *Geoscientific Model Development*, *10*(10), 3715–3743. https://doi.org/10.5194/gmd-10-3715-2017

Vettoretti, G., Ditlevsen, P., Jochum, M., & Rasmussen, S. O. (2022). Atmospheric CO_2 control of spontaneous millennial-scale ice age climate oscillations. *Nature Geoscience*, *15*(4), 1–7. https://doi.org/10.1038/s41561-022-00920-7

Vettoretti, G., & Peltier, W. R. (2016). Thermohaline instability and the formation of glacial north Atlantic super polynyas at the onset of Dansgaard-Oeschger warming events. *Geophysical Research Letters*, *43*(10), 5336–5344. https://doi.org/10.1002/2016gl068891

Vettoretti, G., & Peltier, W. R. (2018). Fast physics and slow physics in the nonlinear Dansgaard–Oeschger relaxation oscillation. *Journal of Climate*, *31*(9), 3423–3449. https://doi.org/10.1175/jcli-d-17-0559.1

Zhang, X., Barker, S., Knorr, G., Lohmann, G., Drysdale, R., Sun, Y., et al. (2021). Direct astronomical influence on abrupt climate variability. *Nature Geoscience*, *14*(11), 819–826. https://doi.org/10.1038/s41561-021-00846-6

Zhang, X., Knorr, G., Lohmann, G., & Barker, S. (2017). Abrupt north Atlantic circulation changes in response to gradual co 2 forcing in a glacial climate state. *Nature Geoscience*, *10*(7), 518–523. https://doi.org/10.1038/ngeo2974

Zhang, X., Lohmann, G., Knorr, G., & Purcell, C. (2014). Abrupt glacial climate shifts controlled by ice sheet changes. *Nature*, *512*(7514), 290–294. https://doi.org/10.1038/nature13592

Zhang, X., & Prange, M. (2020). Stability of the atlantic overturning circulation under intermediate (MIS3) and full glacial (LGM) conditions and its relationship with Dansgaard-Oeschger climate variability. *Quaternary Science Reviews*, *242*, 106443. https://doi.org/10.1016/j.quascirev.2020.106443